

Finite temperature vortex dynamics in Bose Einstein condensates

B. Jackson^{1*}, N. P. Proukakis¹, C. F. Barenghi¹ and E. Zaremba²

¹ *School of Mathematics and Statistics,
University of Newcastle upon Tyne,*

NE1 7RU, United Kingdom,

² *Department of Physics,
Engineering Physics and Astronomy,
Queen's University, Kingston,
Ontario, Canada K7L 3N6,*

(Dated: June 25, 2021)

We study the decay of vortices in Bose-Einstein condensates at finite temperatures by means of the Zaremba-Nikuni-Griffin formalism, in which the condensate is modelled by a Gross-Pitaevskii equation, which is coupled to a Boltzmann kinetic equation for the thermal cloud. At finite temperature, an off-centred vortex in a harmonically trapped pancake-shaped condensate decays by spiralling out towards the edge of the condensate. This decay, which depends heavily on temperature and atomic collisions, agrees with that predicted by the Hall-Vinen phenomenological model of friction force, which is used to describe quantised vorticity in superfluid systems. Our result thus clarifies the microscopic origin of the friction and provides an ab initio determination of its value.

I. INTRODUCTION

The dynamics of Bose-Einstein condensates at finite temperature presents an interesting problem in the study of ultra cold Bose gases. In most experiments, such systems are only partially condensed, with the non-condensed thermal cloud providing a source of dissipation and leading to damping of structures, such as collective modes [1, 2, 3, 4], solitons [5] and vortices [6, 7]. Several approaches have been developed to describe these systems, including generalised mean field treatments [8, 9, 10, 11, 12, 13], number-conserving approaches [14, 15, 16], classical field theory [17, 18, 19], and stochastic approaches [20, 21, 22], as recently reviewed by two of the authors [23], who give a more complete list of references. Although the underlying theory is well understood, the implementation of models which can be actually solved in specific contexts has proven to be a considerable challenge, with the majority of treatments to date assuming the thermal cloud is homogeneous and static.

In this paper we use the formalism of Zaremba, Nikuni and Griffin (ZNG) [10]. The ZNG theory is a kinetic approach in which a generalised Gross-Pitaevskii (GP) equation for the condensate order parameter is coupled to a Boltzmann equation for the thermal cloud. These equations have already been solved numerically [24], and applied to the study of collective modes [25, 26, 27], the hydrodynamic regime [28, 29] and the decay of dark solitons [30], demonstrating good agreement with experiments.

The primary aim of this paper is to apply the ZNG model to quantised vortices at finite temperatures. In a harmonically-trapped condensate at zero temperature a vortex will precess within the condensate, following a trajectory of constant radius, for which the energy remains constant. At finite temperature the presence of dissipation leads to the vortex minimising its energy by moving towards the surface, where it eventually leaves the condensate and disappears.

* Brian Jackson died on 30 August 2007.

This decay has been observed experimentally [6, 7], but the precise theoretical modelling of this process has proven rather challenging.

Our approach should be contrasted with earlier work. Dissipation based on the scattering of single-particle excitations from the mean field potential at the vortex core was considered by Fedichev and Shlyapnikov [31] and was subsequently extended to treat vortex lattices [32, 33]. The problem of vortex nucleation was then considered by Penckwitt *et al.* [37] using an approximation in which the thermal cloud is treated as *static*. Schmidt *et al.* [34] were the first to apply the classical field method to the problem of vortex decay, while more recent applications of the method addressed vortex dynamics in quasi-two-dimensional systems [35, 36]. Duine *et al.* [38] considered the dynamics of a straight vortex line using a closely-related method based on a stochastic Gross-Pitaevskii equation [21] and derived a stochastic equation of motion for the position of the vortex core; a similar equation was also used by Sasik *et al.* to numerically simulate the motion of an isolated vortex in a uniform box with periodic boundary conditions [39]. Compared to the literature cited above, our work represents the first microscopic simulations which fully account for the dynamics of an inhomogeneous thermal cloud.

Our work, however, also has a second motivation. Although the topic of quantised vorticity in superfluids is interesting per se (as shown by the number of recent vortex experiments in atomic Bose–Einstein condensates), it also has implications in the subject of quantum turbulence [40]. Current work on turbulent superfluid ^4He and $^3\text{He-B}$, for example, is concerned with the extent to which turbulence in these systems differs from that found in ordinary classical fluids [41, 42, 43, 44, 45, 46, 47, 48, 49]. What makes quantum fluids attractive from the point of view of understanding the principles of turbulence, is the existence of various forms of dissipation which are distinct from ordinary viscosity. At sufficiently low temperatures, kinetic energy can be dissipated into sound waves, that is phonons [50], via a Kelvin wave cascade [51] or via vortex reconnections [52]. At higher temperatures, the friction force [53] between the superfluid and the normal fluid component can change the nature of the turbulent kinetic energy cascade. For example, in the classical turbulence scenario [54], the Richardson–Kolmogorov inertial cascade is limited at large wavenumbers where viscous dissipation destroys the small scales, whereas in superfluid $^3\text{He-B}$ at relatively high temperatures the friction can limit the inertial cascade at small wavenumbers [55].

The mutual friction between a superfluid and a normal fluid is one of the most intricate issues of superfluidity [56]; in particular, the existence of a transverse force on quantised vortices parametrised by a dimensionless temperature dependence quantity called α' has been controversial [57, 58, 59, 60]. Studying vortex motion in an atomic BEC at finite temperatures, and interpreting the results from the point of view of vortex dynamics, allows one to compute the friction force directly from first principles. This work on an atomic quantum fluid thus provides insights into this important problem which cannot be obtained as readily with superfluid helium.

This paper is structured as follows: Sec. II briefly reviews the ZNG theoretical model and numerical implementation. Sec. III presents our main findings on vortex decay (Sec. III A), high-



FIG. 1: (Colour online) Three-dimensional density isosurface showing an off-centred vortex in a pancake-shaped condensate.

lighting the dependence of the friction coefficients on system parameters (Sec. IIIB), the role of collisions between the atoms (Sec. IIIC), and the effect of thermal cloud rotation (Sec. IIID). Sec. IV presents some concluding remarks and briefly discusses the consequences of our analysis on the motion of vortex lattices.

II. THEORY

A. ZNG formalism

Following Refs [10] and [24], the second-quantised field operator $\hat{\psi}(\mathbf{r}, t)$ can be split into condensate and thermal contributions. Making use of Bose broken symmetry, the full operator is written as $\hat{\psi}(\mathbf{r}, t) = \Psi(\mathbf{r}, t) + \tilde{\psi}(\mathbf{r}, t)$, where $\Psi(\mathbf{r}, t) = \langle \hat{\psi}(\mathbf{r}, t) \rangle$ is the condensate wavefunction (angular brackets denote an expectation value) and $\tilde{\psi}(\mathbf{r}, t)$ is the noncondensate field operator. Starting with the Heisenberg equation of motion for $\hat{\psi}(\mathbf{r}, t)$, one eventually arrives at the following pair of equations:

$$i\hbar \frac{\partial \Psi}{\partial t} = \left(-\frac{\hbar^2 \nabla^2}{2m} + V + gn_c + 2g\tilde{n} - iR \right) \Psi, \quad (1)$$

$$\frac{\partial f}{\partial t} + \frac{\mathbf{p}}{m} \cdot \nabla f - \nabla U \cdot \nabla_{\mathbf{p}} f = C_{12} + C_{22}. \quad (2)$$

Eq. (1) is a generalised Gross–Pitaevskii (GP) equation for the condensate wavefunction $\Psi(\mathbf{r}, t)$, and has been obtained in the so-called ‘Hartree-Fock-Popov’ approximation [8], whereby the static value of the ‘anomalous’ average, which is responsible for certain many-body effects [61, 62, 63, 64], is ignored. Eq. (2) is a Boltzmann equation for the thermal cloud phase space density $f(\mathbf{p}, \mathbf{r}, t)$, with thermal energies calculated in the Hartree-Fock approximation [65]. The condensate density is defined as $n_c = |\Psi|^2$, while the thermal cloud density is obtained from f by means of the momentum integral $\tilde{n} = \int d\mathbf{p}/h^3 f$. The mean field interactions between atoms is parameterised by $g = 4\pi\hbar^2 a/m$, where m is the atomic mass and a is the s-wave scattering length. The thermal atoms experience an effective potential given by $U(\mathbf{r}) = V(\mathbf{r}) + 2g(n_c + \tilde{n})$, where $V(\mathbf{r}) = m(\omega_{\perp}^2 r^2 + \omega_z^2 z^2)/2$ represents the external trap.

The terms involving gn_c and $g\tilde{n}$ in Eq. (1) and ∇U in Eq. (2) represent mean field coupling between atoms in the condensate and the thermal cloud. This coupling is a source of dissipation for the system, and gives rise, for example, to Landau damping of collective modes [66, 67, 68, 69]. The ZNG model also includes ‘collisional integrals’ C_{22} and C_{12} , which respectively denote binary collisions between noncondensate atoms, and between condensate and noncondensate atoms. They are given by:

$$C_{22} = \frac{2g^2}{(2\pi)^5 \hbar^7} \int d\mathbf{p}_2 d\mathbf{p}_3 d\mathbf{p}_4 \delta(\mathbf{p} + \mathbf{p}_2 - \mathbf{p}_3 - \mathbf{p}_4) \delta(\epsilon + \epsilon_2 - \epsilon_3 - \epsilon_4) [(1+f)(1+f_2)f_3f_4 - f f_2(1+f_3)(1+f_4)], \quad (3)$$

$$C_{12} = \frac{2g^2 n_c}{(2\pi)^2 \hbar^4} \int d\mathbf{p}_2 d\mathbf{p}_3 d\mathbf{p}_4 \delta(m\mathbf{v}_c + \mathbf{p}_2 - \mathbf{p}_3 - \mathbf{p}_4) \delta(\epsilon_c + \epsilon_2 - \epsilon_3 - \epsilon_4) [\delta(\mathbf{p} - \mathbf{p}_2) - \delta(\mathbf{p} - \mathbf{p}_3) - \delta(\mathbf{p} - \mathbf{p}_4)] \\ \times [(1+f_2)f_3f_4 - f_2(1+f_3)(1+f_4)], \quad (4)$$

where $f \equiv f(\mathbf{p}, \mathbf{r}, t)$ and $f_i \equiv f(\mathbf{p}_i, \mathbf{r}, t)$. In the above expressions, delta functions enforce momentum and energy conservation in the collisions, where $\epsilon = p^2/(2m) + U$ is the thermal

atom energy (in the Hartree-Fock limit), $\epsilon_c = mv_c^2/2 + \mu_c$ is the local condensate energy, with $\mathbf{v}_c = \hbar(\Psi^*\nabla\Psi - \Psi\nabla\Psi^*)/(2imn_c)$, and μ_c is the chemical potential.

The C_{12} term (4) involves those collisions between condensate and thermal atoms which lead to a transfer of atoms between condensate and thermal cloud. This term is thus related to the source term $-iR\Psi$ appearing in Eq. (1) via

$$R(\mathbf{r}, t) = \frac{\hbar}{2n_c} \int \frac{d\mathbf{p}}{(2\pi\hbar)^3} C_{12}. \quad (5)$$

If R is positive (negative), there is a net local flux of atoms *out of (into)* the condensate.

B. Numerical methods

The methods used for our numerical simulations are discussed more fully in Ref. [24], and are only briefly reviewed here.

Firstly, we must generate a suitable initial state for the simulations which consists of a condensate in equilibrium with a thermal cloud at temperature T . The condensate wavefunction can be obtained by an imaginary time propagation ($t \rightarrow -it$) of (1) with $R = 0$. The thermal cloud density $\tilde{n} = 0$ is first set to zero, and an approximate thermal cloud potential $U \simeq V + 2gn_c$ is constructed from the self-consistently determined condensate wavefunction. This yields the initial thermal cloud density $\tilde{n}_0(\mathbf{r}) = (1/\Lambda^3)g_{3/2}(z)$, where $\Lambda = (2\pi\hbar^2/mk_B T)^{1/2}$ is the thermal de Broglie wavelength, $z(\mathbf{r}) = \exp\{\beta[\mu_c - U(\mathbf{r})]\}$ is the local fugacity and μ_c is the condensate chemical potential. This density is then used in (1) to obtain an improved condensate wavefunction and the procedure is iterated until a self-consistent solution of both the condensate and thermal cloud densities is obtained. (For more details see [24].)

The vortex state of interest in our simulations can be obtained from this equilibrium state by multiplying the condensate wavefunction by the phase factor $\exp[iS(\mathbf{r})]$, where $S(\mathbf{r}) = \arctan((y - y_0)/(x - x_0))$ is the phase profile associated with a straight vortex located at (x_0, y_0) . The GP equation is then solved again in imaginary time for a short period, until a vortex is fully formed in the condensate and most short time scale transients in the initial configuration (for example, phonon excitations) have damped out.

The state generated in this way is a quasi-equilibrium state containing one vortex whose subsequent dynamical evolution is of interest. The generalised Gross-Pitaevskii equation for the condensate wavefunction (1) can be solved readily in real time using standard methods [70], in our case a split-operator Fast Fourier Transform approach on a 3D Cartesian grid. The thermal cloud is described by a swarm of classical test particles, which move in an external potential $U(\mathbf{r}, t)$, and which, during a timestep, can collide with each other or with the condensate. The probabilities of particle collisions are chosen so that they correspond to a Monte Carlo evaluation of the collision integrals in (3) and (4). Together with the Newtonian dynamics of the test particles, this procedure is equivalent to solving the collisional Boltzmann equation (2). The C_{12} probabilities are then summed according to (5) to determine $R(\mathbf{r}, t)$, which appears in the GP equation (1). Since $R(\mathbf{r}, t)$ is a non-Hermitian term, it leads to change in the normalisation of the wavefunction, corresponding to condensate growth or loss, which is accompanied by a compensating removal or creation of thermal particles. An essential ingredient in the simulations is the evaluation of the thermal cloud density $\tilde{n}(\mathbf{r}, t)$, which appears in both (1) and (2) (through the effective potential U). This is achieved by appropriately binning the thermal particles and then convolving the binned distribution with a Gaussian in order to obtain a smoothly varying potential.

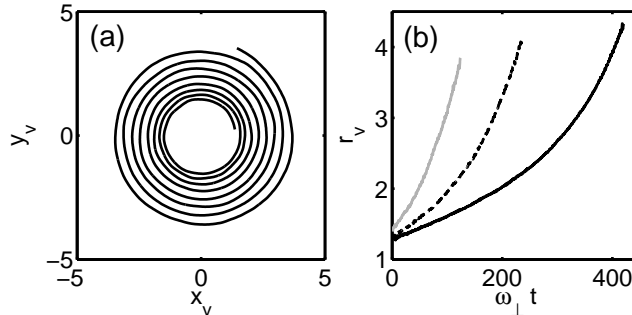


FIG. 2: (a) Position of the vortex (x_v, y_v) (in units of $a_\perp = \sqrt{\hbar/m\omega_\perp}$), as it spirals out of the condensate at $T = 0.7 T_c$. (b) Radial position of the vortex $r_v = \sqrt{x_v^2 + y_v^2}$ as function of time (in units of ω_\perp^{-1}), for $T = 0.5 T_c$ (solid black line), $T = 0.6 T_c$ (dashed black), and $T = 0.7 T_c$ (solid grey).

III. RESULTS

The first simulation to be described is for a pancake-shaped condensate with $N = 10^4$ ^{87}Rb atoms with trap frequencies $\omega_\perp = 2\pi \times 129$ Hz and $\omega_z = \sqrt{8}\omega_\perp$. For these parameters the (ideal gas) critical temperature is $T_c = 177$ nK. This geometry has the advantage that the radius of the condensate in the axial direction is much smaller than in the radial, so that the vortex remains relatively straight throughout its motion. This simplifies the analysis considerably, as the vortex dynamics can be characterised by just its x and y coordinates.

A. Vortex decay

Following the initial preparation phase, the vortex is centred on $x_v(0) \simeq 1.3a_\perp$, $y_v(0) = 0$, as illustrated in Fig. (1), where $a_\perp = \sqrt{\hbar/m\omega_\perp}$ is the harmonic oscillator length in the radial direction. The subsequent vortex position $\mathbf{r}_v(t) = (x_v(t), y_v(t))$ is tracked by finding the corresponding local density minimum in the $z = 0$ plane by means of a quadratic interpolation between grid points. This procedure breaks down when the vortex leaves the bulk of the condensate into the very low densities beyond the edge, so no results are shown when this happens. This condition can be taken as the point at which the vortex “disappears” from the condensate, and would correspond in the experimental context to the density contrast of the vortex being below the detection limit. Since the initialisation process induces a centre-of-mass motion of the condensate, the following analysis depicts the vortex position relative to the centre-of-mass position.

Simulations of the GP equation for $T = 0$ reveal that the vortex precesses in a circular path around the condensate, following a trajectory of constant energy as would be expected for a non-dissipative system. This well-known precessional behaviour can be understood as arising from the non-uniform density of the condensate, which means that the energy of the vortex is a function of its radial position. Hence there is an effective Magnus force, proportional to the gradient of the energy and directed radially, with in turn induces the azimuthal vortex motion [71]. This can be described quantitatively by means of a time-dependent variational method [72, 73, 74]. In addition to the motion described above, the acceleration experienced by the vortex in its circular trajectory can in principle lead to the emission of sound waves. However, for the harmonic confinement being consider, any emission of sound waves is followed by reabsorption, and no net dissipation occurs. There is nevertheless some modulation of the vortex trajectory arising from the dynamical interaction between of the vortex and sound waves [75].

In contrast to this dissipationless motion, the vortex can lose energy at finite temperatures

due to interactions with the thermal component, and as a result, it moves radially towards the condensate edge. The resulting spiral trajectory is illustrated in Fig. 2(a) for a temperature of $T = 0.7T_c$. Fig. 2(b) shows the outward relaxation of the radial position $r_v = |\mathbf{r}_v| = \sqrt{x_v^2 + y_v^2}$ as a function of time. The three curves represent different temperatures, and demonstrate, as one would expect, that the relaxation rate increases with temperature.

As well as monitoring the vortex position, it is instructive to study the evolution of the densities during the simulation. Fig. 3 shows the condensate (top images) and thermal cloud densities (bottom) (cross-sections at $z = 0$) for various times, and for a temperature of $T = 0.7T_c$. The density dip at the vortex core (dark blue) is evident in the condensate images (top), and executes the spiral motion of Fig.2(a). The bottom images show the thermal cloud density; as this is much smaller than the condensate density, a different colour scale is used here for clarity. The thermal cloud density is largest near minima of the effective potential $U(\mathbf{r}, t)$, leading in the present situation to the circular ring of peak thermal cloud density (red) at the edge of the condensate where $n_c \rightarrow 0$. However, the thermal cloud also tends to “fill in” the vortex core since the lower condensate density at this position gives rise to a dip in the effective potential. The resulting peak in the thermal cloud density tends to follow the core as it precesses and spirals out. We note that the stabilisation of the vortex by the thermal cloud suggested in [76] is not observed. It arises when the thermal cloud is treated as *static* [76], but does not occur when the dynamics of the thermal cloud is taken into account.

The radial position of a vortex close to the trap centre exhibits a near-exponential growth in time. This is evident from the inset of Fig. 4, which plots the time evolution of r_v on a logarithmic-linear scale for $T = 0.5T_c$. Deviations from this simple exponential behaviour are observed at later times when the vortex approaches the edge of the condensate; similar behaviour is found for other temperatures. To quantify the relaxation we thus fit $r_v(t)$ over $0 \leq t \leq 50$ to the function $r_v(t) = r_0 \exp(\gamma t)$. The resulting values of γ are plotted in the main panel of Fig. 4 with the black circles.

The departure from a pure exponential behaviour can be interpreted as a position-dependent relaxation rate γ which is enhanced by the local maximum in the thermal atom density near the edge of the condensate (see Fig. 3). To check this interpretation, we performed simulations in which the vortex starts nearer to the centre, e.g. at $r_0 \simeq 0.65a_\perp$, instead of the initial position $r_0 \simeq 1.3a_\perp$ used earlier. The resulting values of γ are plotted as the open circles in Fig. 4, showing smaller values consistent with the lower thermal cloud density closer to the centre of the trap. However, the difference is small, showing that the exponential decay approximation is good until quite near to the condensate edge, where the larger thermal cloud density leads to a more rapid

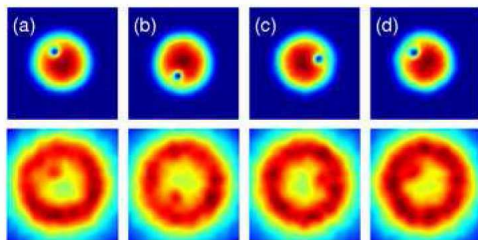


FIG. 3: (Colour online) Density cross-sections of the condensate (top row) and thermal cloud (bottom row) at $z = 0$ for $T = 0.7T_c$, and at the times (a) $\omega_\perp t = 6$, (b) 12 (c) 18, and (d) 24. The colours range from brown/red (high density) to dark blue (low density), with different scales for the condensate and thermal cloud densities.

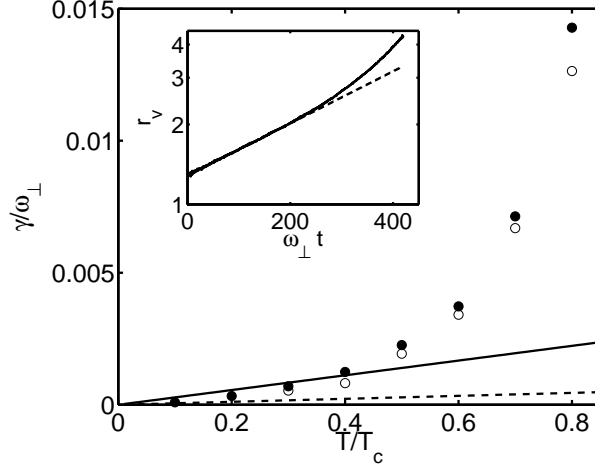


FIG. 4: (Inset) Lin-log plot of the vortex radial position as a function of time, for $T = 0.5 T_c$ (solid line). The dashed line is an exponential fit, $r_v(t) = r_0 e^{\gamma t}$, to the data over $0 \leq t \leq 50$. The main figure plots the resulting values of γ for an initial vortex position of $r_0 \simeq 1.3$ (solid circles) and $r_0 \simeq 0.65$ (open circles). For comparison, the solid and dashed lines plot the results of FS [31] and DLS [38] respectively.

relaxation (inset of Fig. 4).

It is of interest to compare our results to existing analytical predictions obtained by Fedichev and Shlyapnikov (FS) [31], and Duine, Leurs and Stoof (DLS) [38]. Both FS and DLS actually quote the timescale τ for the decay of a vortex from position r_{\min} to r_{\max} , but this can be converted to a decay rate using $\tau = \gamma^{-1} \ln(r_{\max}/r_{\min})$. In both of these works the decay of the vortex is found to be exponential, with a rate $\gamma \propto T$ but with different proportionality coefficients due to the different approximations made in the two theories (see below for the role of the noise term in the DLS analysis). These rates are displayed in Fig. 4 by solid (FS) and dashed lines (DLS). It is apparent that the rates found by FS are comparable to ours at the lower temperatures, but differ significantly at higher T due to the stronger (approximately quadratic) temperature dependence found in our simulations.

FS assumed a uniform condensate in a cylindrical container, and modelled the decay solely as the result of mean-field interactions. The DLS study on the other hand, includes the important C_{12} collisional coupling between the condensate and thermal cloud. With the aim of obtaining analytical results, they approximate the condensate density profile by a Gaussian which is reasonably accurate for the most relevant region near the center of the trap [77]. In this regard, it should be noted that such an approximation has been shown to produce correct results for the frequencies of collective modes even for Thomas-Fermi condensates [78]. Our present simulations, which include both mean field and collisional coupling mechanisms, enable us to assess their relative importance, which will be discussed in Sec. III C. More importantly, our simulations differ from these approaches in that they are actually performed for a dynamical thermal cloud, with both the condensate and thermal cloud densities determined self-consistently during the simulations.

For completeness, we should however make two additional remarks regarding the DLS approach. Firstly, in their preceding work [78], Duine and Stoof argued that enhanced damping of collective modes at higher temperatures could be related to the position dependence of the self-energy (and hence of the damping term $-iR\Psi$), which was ignored in their analytical treatment based on a volume average over the size of the condensate. In the present context, this could partly account [79] for a deviation of the computed damping rate γ/ω_{\perp} at higher temperatures from the linear behaviour seen in Fig. 4. Although such simulations have not been performed to date, the resulting

corrections are likely to be smaller than the observed disagreement, whose origin we believe lies primarily in the dynamics of the thermal cloud.

On the other hand, the DLS analysis is actually more general than ours in that it contains an additional noise term in the equation of motion of the vortex. This provides stochastic “kicks” to the vortex and the ensuing Brownian motion allows for the migration of a vortex away from the centre of the trap. Were it not for the noise, a centred vortex would have an infinite lifetime. This would be the case in an exact application of the ZNG theory. However, its numerical implementation in terms of discrete test particles does introduce statistical fluctuations in the thermal cloud density which plays the role of noise. Thus we indeed find in simulations of a centred vortex a finite, albeit long, lifetime ($\omega_{\perp}\tau \simeq 1000$ for the relatively high temperature of $T = 0.7T_c$ as compared to $\omega_{\perp}\tau \simeq 120$ for $r_v(0) \simeq 1.3a_{\perp}$). This long lifetime, however, should not be taken seriously since it depends on the actual number of test particles used in the simulations. The simulation nevertheless makes clear that this ‘numerical noise’ is of secondary importance at larger radii where the direct coupling to the thermal cloud is the dominant dissipative effect. Although it is something to be checked, it is unlikely that the stochastic term makes a significant contribution to the spiralling out of a vortex when it is located far from the trap centre.

Finally, it is worth remarking that our computed decay rates (from approximately 0.5 s^{-1} to 3 s^{-1} in the range $T/T_c = 0.4$ to 0.6) are in order-of-magnitude agreement with the decay rates observed for a vortex lattice [7] (approximately 0.3 s^{-1} to 3 s^{-1} over the same relative range).

B. Friction coefficients

In order to further understand the origin of this exponential decay, it is instructive to consider the two-fluid hydrodynamics model used to describe superfluid liquid helium [80]. In this context, dissipation arises from the interaction between the quantised vortices and the thermal excitations (phonons and rotons) which form the normal fluid [53, 81]. Since the radius of the superfluid vortex core is much smaller than the typical separation between vortices or any other length scale of interest in the flow, the vortex is described in parametric form as a three-dimensional space curve $\mathbf{s} \equiv \mathbf{s}(\xi, t)$, where ξ is the arclength. The resulting equation of motion [82] is:

$$\frac{d\mathbf{s}}{dt} = \mathbf{v}_s + \mathbf{v}_i + \alpha \mathbf{s}' \times (\mathbf{v}_n - \mathbf{v}_s - \mathbf{v}_i) - \alpha' \mathbf{s}' \times [\mathbf{s}' \times (\mathbf{v}_n - \mathbf{v}_s - \mathbf{v}_i)], \quad (6)$$

where $\mathbf{s}' = d\mathbf{s}/d\xi$ is the unit tangent along the vortex at the position \mathbf{s} , \mathbf{v}_s is any imposed superfluid velocity, \mathbf{v}_n is the normal fluid velocity, and \mathbf{v}_i is the self-induced velocity of the vortex arising from its own curvature, the presence of other vortices, and any inhomogeneity of the fluid. The first two terms on the right hand side of Eq. (6) state that at $T = 0$ the vortex is advected by the local superflow $\mathbf{v}_s + \mathbf{v}_i$. The remaining two terms reflect the fact that, at nonzero T , the normal fluid streaming past the vortex core exerts a force per unit length whose intensity is controlled by the temperature-dependent friction coefficients α and α' [53, 83, 84].

In turbulent helium, the friction coefficients α and α' play a key role because they account for the mutual friction between the superfluid and the normal fluid and control the transfer of energy between the two fluids at various length scales and hence the nature of the inertial range cascade [42, 88]. The first coefficient, α , describes dissipative effects and leads, for example, to the shrinking [53] of a vortex ring or the damping of a Kelvin wave [85] in a normal fluid at rest. In the case of rotating helium, α determines the attenuation of second sound waves, so it allows the experimentalist to determine the density of vortex lines [86]. The second coefficient, α' , is not dissipative, and, in rotating helium, splits a second sound resonance (besides the classical rotational splitting) in a suitably designed cavity [87]. It has been argued [89, 90] that the ratio of inertial

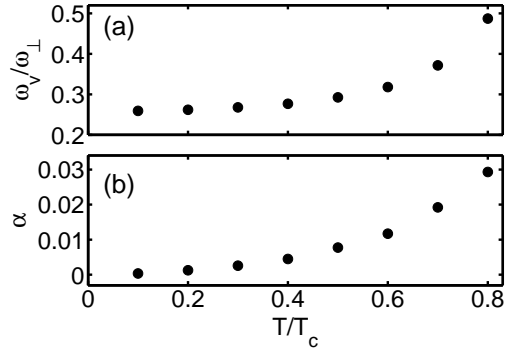


FIG. 5: (a) Precession angular frequency of the vortex, ω_v , as a multiple of the radial trap frequency ω_\perp . (b) Friction coefficient α as a function of relative temperature T/T_c , for $N = 10^4$ and a pancake trap geometry $\omega_z/\omega_\perp = \sqrt{8}$.

and dissipative forces, which is called the Reynolds number in the case of ordinary turbulence [54], is simply $\alpha/(1 - \alpha')$ in the case of quantum turbulence.

In our case of a pancake-shaped condensate the vortex line remains approximately straight, so we can then replace \mathbf{s} by the vortex position \mathbf{r}_v , while $\mathbf{s}' = \hat{\mathbf{z}}$. Both the condensate and thermal cloud are stationary, and so $\mathbf{v}_s = \mathbf{v}_n = 0$. This just leaves \mathbf{v}_i , which in this case corresponds to the azimuthal vortex motion induced by the inhomogeneity of the condensate at zero T (hence, $\mathbf{v}_i = v_i \hat{\phi}$). Rewriting Eq. (6) in cylindrical polar coordinates gives for the azimuthal component

$$\omega_v = (1 - \alpha') \frac{v_i}{r_v}, \quad (7)$$

where $\omega_v = \dot{\phi}_v$ is the vortex precession frequency at finite T and the dot denotes a time derivative.

To a first approximation we ignore the mutual friction coefficient α' . We then find $\omega_v = v_i/r_v$, and thus obtain for the radial component

$$\frac{dr_v}{dt} = \alpha \omega_v r_v. \quad (8)$$

If α and ω_v are constant, then one simply recovers the exponential behaviour discussed in the previous section, with $\gamma = \alpha \omega_v$.

In actual fact, α and ω_v would not be expected to be constant during the course of the vortex decay. The condensate and thermal cloud are both non-uniform (implying a dependence of α on position), while ω_v is only constant near the centre, and increases as the vortex approaches the edge [71]. However, from the evidence of Fig. 4 (inset), Eq. (8) is a good approximation for times when the vortex is close to the centre where the densities are relatively uniform.

Values of α can therefore be estimated from γ in Fig. 4. The other necessary ingredient is ω_v , which can be calculated as a function of time using $\omega_v = x_v \dot{y}_v - y_v \dot{x}_v$, where numerically the time derivatives are calculated using central differences. Due to errors in locating the vortex position, there are large fluctuations in the calculated ω_v . To obtain the corresponding values we thus average results over 2 – 3 orbits of the vortex, corresponding to times $0 < \omega_\perp t < 50$. The resulting mean values are plotted in Fig. 5 (a). These results are also used for calculating the values of α presented in Fig. 5 (b). The observed increase in α with rising T is similar to the behaviour observed in liquid ^3He [84] and ^4He [53, 83], and is consistent with results obtained using the related but simpler phenomenologically damped GP equation [91].

Let us now investigate the role of the α' coefficient in Eq. (6). Experiments in liquid helium show a small effect, and there has been some controversy in the literature about this transverse

component of the friction force [57, 58, 59, 60]. This issue can *be addressed* within our simulations by comparing the “dynamic” thermal cloud frequency ω_v to a “static” value ω_{st} found using a GP simulation in which the dynamics of the thermal cloud is ignored, that is, it retains its initial equilibrium form for all times. In this *static thermal cloud approximation*, the thermal cloud exerts a time-independent mean-field potential on the condensate, and its effect can be identified with the v_i/r_v term in Eq. (7), giving the simple relation for $\alpha' = (1 - \omega_v/\omega_{st})$. We find that ω_v and ω_{st} are equal to within 2 – 3 %, showing that the changes observed in ω_v in Fig. 5 are almost entirely due to the effects of the static thermal cloud potential on the condensate density profile, and not to “real” dynamical effects of finite temperatures. The errors in measuring the vortex precession frequency are such that we cannot confidently extract a value for α' , although our simulations indicate that $|\alpha'| < 0.02$ throughout the measured temperature range $0 < T/T_c < 0.8$. This agrees with recent results of Berloff and Youd [92] obtained by means of classical field theory.

We also explore the dependence of these parameters on the total number of atoms, N . Fig. 6 shows results for N between 10^4 and 10^5 , and a fixed value of $T = 0.5T_c$. The decay rate γ , plotted in Fig. 6 (a), tends to decrease with increasing N . The vortex precession frequency shown in Fig. 6 (b) also has this decreasing trend, in agreement with what one would expect from GP solutions. These decreasing trends approximately cancel when calculating $\alpha = \gamma/\omega_v$, leading to variations having no clear dependence on N . The scatter reflects the uncertainty in the calculation of α and suggests that this parameter is approximately independent of atom number.

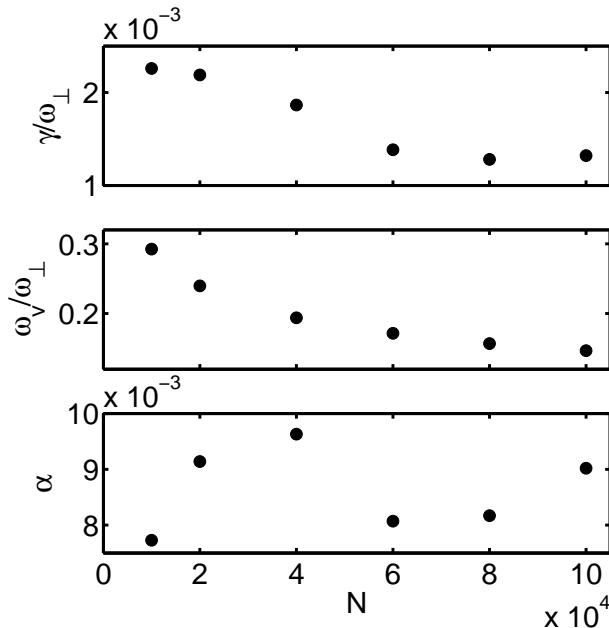


FIG. 6: (a) Decay rate γ , (b) precession frequency ω_v , and (c) α , as a function of total number of atoms N , for temperature $T/T_c = 0.5$ and a pancake geometry.

C. Collisionless simulations

In general, damping in the ZNG formalism arises from the coupling of the condensate to the thermal cloud by means of mean field interactions and C_{12} collisions. In order to explore the relative importance of these two contributions, we have performed simulations where collisions are not present, so $C_{12} = C_{22} = 0$ in (2), and the only source of dissipation is mean-field coupling.

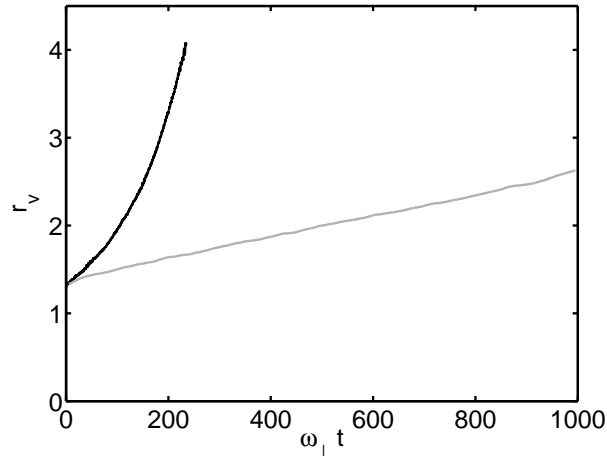


FIG. 7: Radial position of the vortex *vs.* time for $T = 0.6 T_c$, and collisional (black line), and collisionless (grey line) simulations.

Physically, this dissipation is a form of Landau damping whereby the motion of the vortex core through the thermal cloud generates thermal excitations [69]. In Fig. 7 the radial position for the collisionless simulation at $T = 0.6 T_c$ is shown as the grey line, and compared to the collisional result in black. Without collisions one obtains a much slower decay, highlighting the crucial role of collisional damping in the simulations, a conclusion which has been numerically verified over a broad range of temperatures. The near linear variation of r_v with time seen in Fig. 7 indicates that an exponential function would be a poor fit to the data in this case. In view of Eq. (8), it would appear that the mean-field contribution to α must be a decreasing function of r_v , but we have no simple explanation for this.

D. Rotating thermal clouds

We also consider the case where, instead of being stationary initially, the thermal cloud undergoes solid-body rotation around the z -axis with angular frequency Ω_{th} . The thermal cloud velocity at the vortex core is then $\mathbf{v}_n = \Omega_{\text{th}} r_v \hat{\phi}$. Hence $\Omega_{\text{th}} > 0$ represents rotation in the same sense as the vortex precession, while $\Omega_{\text{th}} < 0$ indicates rotation in the opposite sense. Using Eq. (6) then yields:

$$\omega_v = (1 - \alpha') \frac{v_i}{r_v} + \alpha' \Omega_{\text{th}}, \quad (9)$$

and,

$$r_v = r_0 e^{\alpha(\omega_v - \Omega_{\text{th}})t}. \quad (10)$$

For these simulations we start with the equilibrium condensate and thermal cloud distributions evaluated at $T = 0.7 T_c$ and $\Omega_{\text{th}} = 0$. A rigid body rotation of the thermal cloud is then imposed by adding $\mathbf{v}_n = \Omega_{\text{th}} r_v \hat{\phi}$ to each atom's velocity. It should be noted that the thermal cloud will now no longer be in "equilibrium" since there is a centrifugal effect which tends to expand the cloud. This initial outward expansion leads to an oscillation in the radial direction and, since angular momentum is conserved, a corresponding oscillation of the cloud's angular velocity.

The vortex decay curves are plotted in Fig. (8) for different Ω_{th} , and show that the decay rate increases for rotations opposite to the vortex precession direction ($\Omega_{\text{th}} = -0.2$), but decreases when

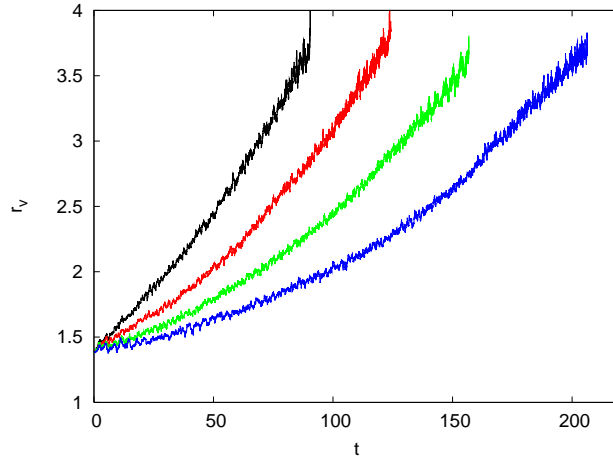


FIG. 8: (Colour online). Time evolution of vortex radial position for $T = 0.7 T_c$ and a rotating thermal cloud. The different curves represent varying thermal cloud rotation rates, with $\Omega_{\text{th}} = -0.2$ (black, top), $\Omega_{\text{th}} = 0$ (red), $\Omega_{\text{th}} = 0.2$ (green), and $\Omega_{\text{th}} = 0.37$ (blue, bottom).

they rotate in the same direction ($\Omega_{\text{th}} = 0.2$ and $\Omega_{\text{th}} = 0.37$). This is consistent with the expected behaviour from Eq. (10). To study the problem more quantitatively, we again fit exponentials of the form ae^{bt} to the decay curves over $0 \leq \omega_{\perp} t \leq 50$. The values of b for the different Ω_{th} are plotted in Fig. 9. The straight line is the expected result from (10), $b = \alpha(\omega_v - \Omega_{\text{th}})$, where α and ω_v are taken from the results of the $\Omega_{\text{th}} = 0$ simulations found earlier. Our results are in quite good agreement with this behaviour, although some small discrepancies are apparent. These could be due to the oscillations in Ω_{th} noted earlier, whereas Eq. (10) assumes that Ω_{th} is strictly time-independent throughout the precessional motion of the vortex.

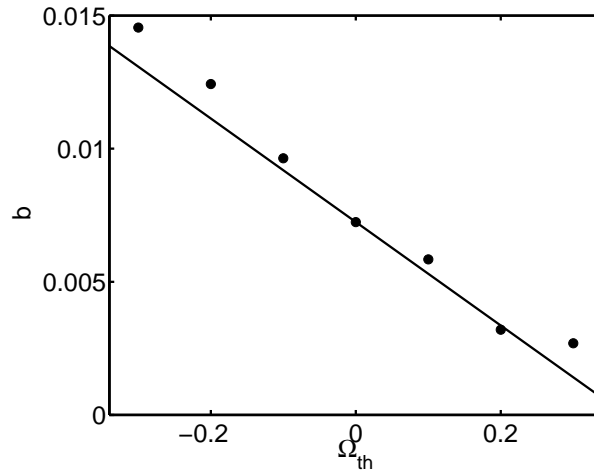


FIG. 9: Value of decay rate γ for different rotation rates of the thermal cloud, Ω_{th} . The solid line plots the function $\gamma = \gamma_0(1 - \Omega_{\text{th}}/\omega_{v0})$ (where γ_0 and ω_{v0} are the decay rate and the precession angular velocity respectively for a non-rotating thermal cloud), which is the expected dependence from Eq. (10).

IV. CONCLUSIONS

In summary, we have studied the finite temperature dynamics of a single vortex in a partially-condensed ultra-cold Bose gas. Our methodology and detailed simulations provide several advantages over previous studies. Firstly, our simulations include the full effects of the trapping potential through the self-consistent determination of condensate and thermal cloud in the initial state. This results in a more realistic model as compared to those using the approximation of uniform densities [31, 37, 38]. The inclusion of non-uniform densities accounts more realistically for both the dynamics of the vortex and the positional dependence of the dissipation. Secondly, our model includes both mean-field [31] and collisional [38] damping, and allows us to compare the relative importance of the two mechanisms. Thirdly, the thermal cloud is not assumed to be static as in earlier treatments, but is treated dynamically on the same footing as the condensate. This more refined treatment negates suggestions that the thermal cloud can act as a “pinning potential”, stabilising the vortex [76]. In addition, it has allowed us to observe the change in damping when the thermal cloud is moving relative to the condensate as, for example, when undergoing a rotation.

We also compared our results for the vortex relaxation rate to those of other studies and found some significant differences, particularly with regard to its temperature dependence. Furthermore, by comparing the trajectory of vortices with the predictions of phenomenological vortex dynamics equations, we were able to determine the mutual friction coefficients from first principles.

Our approach can also be extended to study the role of a dynamical thermal cloud on vortex lattice dynamics [93, 94, 95], thereby complementing and extending existing work [32, 33, 37, 76, 96, 97, 98, 99]. To illustrate this possibility, we conclude by briefly reporting on some preliminary results for the decay of vortex lattices. We consider the evolution of two different vortex lattice configurations shown in Fig. 10. Both vortex arrays initially contain seven vortices (left images), however they differ in the way the vortices are arranged. The first array (top images) consists of one vortex at the centre of the condensate and a ring of six vortices around it, whereas the second array (bottom) consists of a ring of seven vortices with no central vortex. These arrays rotate in the laboratory frame, and at finite temperatures, the effects of dissipation lead to the gradual disappearance of the off-centred vortices, one by one. For simulations performed at $T = 0.7T_c$, we find that the array with all vortices arranged in a ring decays faster: after the first six vortices have decayed, the system is left with a single off-centre vortex which moves relatively rapidly to the edge and disappears. This whole evolution occurs on a time scale $\omega_{\perp}t \approx 150$. The decay rate is in order-of-magnitude agreement with measurements performed with a bigger lattice [7] after the latter are extrapolated to our value of T/T_c .

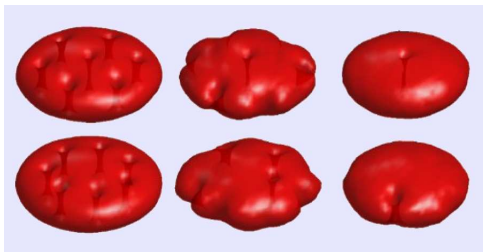


FIG. 10: (Colour online). Vortex lattice decay at $T = 0.7 T_c$. The top row shows the time evolution (left to right) of a lattice with a vortex initially at the centre; the bottom row shows the evolution of a lattice with the same number of vortices but having a ring configuration.

In contrast to this, the lattice with the central vortex reaches a point where a single metastable central vortex remains after the other six have been shed. This vortex also eventually decays,

but our simulations suggest that the decay occurs on a much longer timescale. Some numerical experiments we have performed for configurations with no initial central vortex have exhibited a similar metastable behaviour. If, during the initial part of the evolution (in which the vortices move irregularly), a vortex ends up sufficiently close to the centre, it can become “stuck” near the centre while the other vortices are shed. These observations are in agreement with reports [100] that the decay time of the last vortex is much longer than that of the initial vortex array.

We stress, however, that a more accurate treatment of the evolution of a metastable central vortex requires the explicit inclusion of stochastic noise to provide a “kick”, as discussed in [38, 39]. Such a term was included in a recent discussion [99], however the thermal cloud was still treated as static. A combination of the stochastic Gross-Pitaevskii equation and the quantum Boltzmann equation may thus be needed to provide a more complete description of this particular situation. However, we expect that most other cases can be modelled extremely well by the Zaremba - Nikuni-Griffin approach. In particular, it would of interest to see if more detailed calculations of vortex lattice decay would be consistent with experimental observations [7]. Other applications might include the study of vortex lattice excitations (Tkachenko modes) [101], and the dynamics of bent vortices in elongated condensates [6].

This work was funded by EPSRC grant EP/D040892/1 (BJ, NPP, CFB) and by NSERC of Canada (EZ).

-
- [1] D. S. Jin, M. R. Matthews, J. R. Ensher, C. E. Wieman, and E. A. Cornell, Phys. Rev. Lett. **78**, 764 (1997).
 - [2] D. M. Stamper-Kurn, H.-J. Miesner, S. Inouye, M. R. Andrews, and W. Ketterle, Phys. Rev. Lett. **81**, 500 (1998).
 - [3] O. Maragò, G. Hechenblaikner, E. Hodby, C. J. Foot, Phys. Rev. Lett. **86**, 3938 (2001).
 - [4] F. Chevy, V. Bretin, P. Rosenbusch, K. W. Madison, and J. Dalibard, Phys. Rev. Lett. **88**, 250402 (2002).
 - [5] S. Burger *et al.*, Phys. Rev. Lett. **83**, 5198 (1999).
 - [6] P. Rosenbusch, V. Bretin, and J. Dalibard, Phys. Rev. Lett. **89**, 200403 (2002).
 - [7] J. R. Abo-Shaeer, C. Raman, and W. Ketterle, Phys. Rev. Lett. **88**, 070409 (2002).
 - [8] A. Griffin Phys. Rev. B **53**, 9341 (1996).
 - [9] N. P. Proukakis and K. Burnett, J. Res. Natl. Inst. Stand. Technol. **101** 457 (1996); N. P. Proukakis, J. Phys. B **34**, 4737 (2001).
 - [10] E. Zaremba, T. Nikuni, and A. Griffin, J. Low. Temp. Phys. **116**, 277 (1999).
 - [11] R. Walser, J. Williams, J. Cooper and M. Holland, Phys. Rev. A **59**, 3878 (1999); R. Walser, J. Cooper and M Holland, Phys. Rev. A **63**, 013607 (2000).
 - [12] M. Imamovic-Tomasovic and A. Griffin, Phys. Rev. A **60**, 494 (1999).
 - [13] M. J. Bijlsma, E. Zaremba and H. T. C. Stoof, Phys. Rev. A **62**, 063609 (2000).
 - [14] C. W. Gardiner, Phys. Rev. A **56**, 1414 (1997).
 - [15] Y. Castin and R. Dum, Phys. Rev. A **57**, 3008 (1998).
 - [16] S. A. Morgan, J. Phys. B **33**, 3847 (2000); S. A. Gardiner and S. A. Morgan, Phys. Rev. A **75**, 043621 (2007).
 - [17] B. V. Svistunov, J. Mosc. Phys. Soc. **1**, 373 (1991); Y. Kagan and B. V. Svistunov, Phys. Rev. Lett. **79**, 3331 (1997) and Sov. Phys. JETP **75**, 387 (1992).
 - [18] M. J. Davis, S. A. Morgan and K. Burnett, Phys. Rev. Lett. **87**, 160402 (2001); P. B. Blakie and M. J. Davis, Phys. Rev. A **72**, 063608 (2005).
 - [19] M. Brewczyk, M. Gajda and K. Rzazewski, J. Phys. B **40**, R1 (2007).
 - [20] C. W. Gardiner and P. Zoller, Phys. Rev. A **58**, 536 (1998); C. W. Gardiner and P. Zoller, Phys. Rev. A **61**, 033601 (2000).

- [21] H.T.C. Stoof, Phys. Rev. Lett. **78**, 768 (1997); H. T. C. Stoof, J. Low J Temp. Phys. **114**, 11 (1999); H. T. C. Stoof and M. J. Bijlsma, J. Low Temp. Phys. **124**, 431 (2001).
- [22] C.W. Gardiner, J.R. Anglin and T.I.A. Fudge, J. Phys. B **35**, 1555 (2002); C. W. Gardiner and M. J. Davis, J. Phys B **36**, 4731 (2003).
- [23] N.P. Proukakis and B. Jackson, to appear in J. Phys. B (2008).
- [24] B. Jackson and E. Zaremba, Phys. Rev. A **66**, 033606 (2002).
- [25] B. Jackson and E. Zaremba, Phys. Rev. Lett. **87**, 100404 (2001).
- [26] B. Jackson and E. Zaremba, Phys. Rev. Lett. **88**, 180402 (2002).
- [27] B. Jackson and E. Zaremba, Phys. Rev. Lett. **89**, 150402 (2002).
- [28] T. Nikuni and A. Griffin, Phys. Rev. A **63**, 033608 (2001).
- [29] T. Nikuni and A. Griffin, Phys. Rev. A **69**, 023604 (2004).
- [30] B. Jackson, N. P. Proukakis, and C. F. Barenghi, Phys. Rev. A **75**, 051601(R) (2007).
- [31] P. O. Fedichev and G. V. Shlyapnikov, Phys. Rev. A **60**, R1779 (1999).
- [32] O. N. Zhuravlev, A. E. Muryshev, and P. O. Fedichev, Phys. Rev. A **64**, 053601 (2001).
- [33] P. O. Fedichev and A. E. Muryshev, Phys. Rev. A **65**, 061601(R) (2002).
- [34] H. Schmidt, K. Góral, F. Floegel, M. Gajda, and K. Rzążewski, J. Opt. B: Quantum Semiclass. Opt. **5**, S96 (2003).
- [35] Z. Hadzibabic, P. Krüger, M. Cheneau, B. Battelier and J. Dalibard, Nature (London) **441**, 1118 (2006).
- [36] T. P. Simula and P. B. Blakie, Phys. Rev. Lett. **96**, 020404 (2006); T. P. Simula, M. J. Davis and P. B. Blakie, Phys. Rev. A **77**, 023618 (2008).
- [37] A. A. Penckwitt, R. J. Ballagh and C. W. Gardiner, Phys. Rev. Lett. **89**, 260402 (2002).
- [38] R. A. Duine, B. W. A. Leurs, and H. T. C. Stoof, Phys. Rev. A **69**, 053623 (2004).
- [39] R. Šášik, L. M. A. Bettencourt, and S. Habib, Phys. Rev. B **62**, 1238 (2000).
- [40] *Quantized Vortex Dynamics and Superfluid Turbulence*, Springer, Berlin (2001), edited by C.F. Barenghi, R.J. Donnelly and W.F. Vinen.
- [41] J. Maurer, and P. Tabeling, Europhysics Lett. **43**, 29 (1998).
- [42] W.F. Vinen and J.J. Niemela, J. Low Temp. Phys. **128**, 167 (2002).
- [43] T.V. Chagovets, A.V. Gordeev and L. Skrbek, Phys. Rev. E **76** 027301 (2007).
- [44] C.F. Barenghi, to appear in Physica D.
- [45] D.I. Bradley, D.O. Clubb, S.N. Fisher, A.M. Guenault, R.P. Haley, C.J. Matthews, G.R. Pickett, V. Tsepelin and K. Zaki, Phys. Rev. Lett. **96**, 035301 (2006).
- [46] M. Tsubota, T. Araki and C. F. Barenghi, Phys. Rev. Letters **90**, 205301 (2003).
- [47] V. B. Eltsov, A. P. Finne, R. Hanninen, J. Kopu, M. Krusius, M. Tsubota, and E. V. Thuneberg, Phys. Rev. Lett. **96**, 215302 (2006)
- [48] T. Lipniacki, European J. Mechanics B/Fluids **25**, 435 (2006)
- [49] D. Kivotides, Phys. Rev. B **76**, 054503 (2007)
- [50] D.C. Samuels and C.F. Barenghi, Phys. Rev. Lett. **81**, 4381 (1998).
- [51] D. Kivotides, J.C. Vassilicos, D.C. Samuels and C.F. Barenghi, Phys. Rev. Lett. **86**, 3080 (2001); W.F. Vinen, M. Tsubota and A. Mitani, Phys. Rev. Lett. **91**, 135301 (2003); E. Kozik and B. Svistunov, Phys. Rev. Lett. **92** 035301 (2004); S. Nazarenko, JETP Lett. **84**, 585 (2007).
- [52] M. Leadbeater, T. Winiecki, D.C. Samuels, C.F. Barenghi and C.S. Adams, Phys. Rev. Lett. **86**, 1410 (2001); C.F. Barenghi and D.C. Samuels, J. Low Temp. Physics **36**, 281 (2004).
- [53] C. F. Barenghi, W. F. Vinen and R. J. Donnelly, J. Low Temp. Physics **52**, 189 (1982).
- [54] U. Frisch *Turbulence*, Cambridge University Press (1995).
- [55] W.F. Vinen, Phys. Rev. B **71**, 024513 (2005).
- [56] E.B. Sonin, Rev. Modern Phys. **59** 87 (1987).
- [57] S.V. Iordanskii, Sov. Phys. JETP **22**, 160 (1966).
- [58] E.B. Sonin, Sov. Phys. JETP **42**, 469 (1975).
- [59] E.B. Sonin, Phys. Rev. B **55**, 485 (1997).
- [60] P. Ao and D. J. Thouless, Phys. Rev. Lett. **70** 2158 (1993).
- [61] H. T. C. Stoof, M. Bijlsma and M. Houbiers, J. Res. Natl. Inst. Stand. Technol. **101**, 443 (1996); M. Bijlsma and H. T. C. Stoof, Phys. Rev. A **55**, 498 (1997).
- [62] N. P. Proukakis, S. A. Morgan, S. Choi and K. Burnett, Phys. Rev. A **58**, 2435 (1998).
- [63] H. Shi and A. Griffin, Phys. Rep. **304**, 1 (1998).

- [64] D. A. W. Hutchinson, K. Burnett, R. J. Dodd, S. A. Morgan, M. Rusch, E. Zaremba, N. P. Proukakis, M. Edwards and C. W. Clark, *J. Phys. B* **33**, 3825 (2000).
- [65] F. Dalfovo, S. Giorgini, L. P. Pitaevskii, and S. Stringari, *Rev. Mod. Phys.* **71**, 463 (1999).
- [66] L. P. Pitaevskii and S. Stringari, *Phys. Lett.* **235**, 398 (1997).
- [67] S. Giorgini, *Phys. Rev. A* **57**, 2949 (1998).
- [68] M. Guilleumas and L. P. Pitaevskii, *Phys. Rev. A* **61**, 013602 (1999).
- [69] B. Jackson and E. Zaremba, *New J. Phys.* **5**, 88 (2003).
- [70] A. Minguzzi, S. Succi, F. Toschi, M. P. Tosi, and P. Vignolo, *Phys. Rep.* **395**, 223 (2004).
- [71] B. Jackson, J. F. McCann, and C. S. Adams **61**, 013604 (1999).
- [72] A. A. Svidzinsky and A. L. Fetter, *Phys. Rev. Lett.* **84**, 5919 (2000).
- [73] E. Lundh and P. Ao, *Phys. Rev. A* **61**, 063612 (2000).
- [74] A. L. Fetter and J.-k. Kim, *J. Low Temp. Phys.* **125**, 239 (2001).
- [75] N.G. Parker, N.P. Proukakis, C.F. Barenghi and C.S. Adams, *Phys. Rev. Lett.* **92**, 160403 (2004).
- [76] S. M. M. Virtanen and M. M. Salomaa, *J. Phys. B* **35**, 3967 (2002).
- [77] H.T.C. Stoof (Private Communication)
- [78] R.A. Duine and H.T.C. Stoof, *Phys. Rev. A* **65**, 013603 (2001).
- [79] R.A. Duine (Private Communication)
- [80] R. J. Donnelly, *Quantized Vortices in Helium II*, Cambridge University Press, Cambridge (1991).
- [81] H. E. Hall, and W. F. Vinen, *Proc. Roy. Soc. A* **238**, 215 (1956).
- [82] K. W. Schwarz, *Phys. Rev. B* **38**, 2398 (1988).
- [83] R.J. Donnelly and C.F. Barenghi, *J. Phys. Chem. Ref. Data* **27**, 1217 (1998)
- [84] T.D.S. Bevan et al., *J. Low Temp Phys.* **109**, 423 (1997).
- [85] C.F. Barenghi, R.J. Donnelly and W.F. Vinen, *Phys. Fluids* **28**, 498-504 (1985).
- [86] C. F. Barenghi, A. V. Gordeev and L. Skrbek, *Phys. Rev. E* **74**, 026309 (2006).
- [87] P. Lucas, *J. Phys. C* **3**, 1180 (1970).
- [88] C. F. Barenghi, S. Hulton and D. C. Samuels, *Phys. Rev. Letters* **89** 275301 (2002).
- [89] A.P. Finne, T. Araki, R. Blaauwgeers, V.B. Eltsov, N.B. Kopnin, M. Krusius, L. Skrbek, M. Tsubota and G.E. Volovik, *Nature* **424** 1022 (2003).
- [90] A.P. Finne, S. Boldarev, V.B. Eltsov and M. Krusius, *J. Low Temp. Phys.* **138**, 567 (2005).
- [91] E.J.M. Madarassy and C.F. Barenghi, *J. Low Temp. Phys.* **152** 122 (2008).
- [92] N.G. Berloff and A.J. Youd, *Phys. Rev. Lett.* **99**, 145301 (2007).
- [93] K. W. Madison, F. Chevy, W Wohlleben and J. Dalibard, *Phys. Rev. Lett.* **84**, 806 (2000).
- [94] J. R. Abo-Shaer, C. Raman, J. M. Vogels and W. Ketterle, *Science* **292**, 476 (2001).
- [95] E. Hodby, G. Hechenblaikner, S.A. Hopkins, O.M. Marago and C.J. Foot, *Phys. Rev. Lett.* **88**, 010405 (2001).
- [96] C. Lobo, A. Sinatra and Y. Castin, *Phys. Rev. Lett.* **92**, 020403 (2004).
- [97] M. Tsubota, K. Kasamatsu and M. Ueda, *Phys. Rev. A* **65**, 023603 (2002); K. Kasamatsu, M. Machida, N. Sasa and M. Tsubota, *Phys. Rev. A* **71**, 063616 (2005).
- [98] S. M. M. Virtanen, T. P. Simula and M. M. Salomaa, *Phys. Rev. Lett.* **86**, 2704 (2001).
- [99] A.S. Bradley, C.W. Gardiner and M.J. Davis, *Phys. Rev. A* **77**, 033616 (2008).
- [100] V. Bretin, P. Rosenbusch, F. Chevy, G. V. Shlyapnikov and J. Dalibard, *Phys. Rev. Lett.* **90**, 1004031 (2003).
- [101] I. Coddington, P. Engels, V. Schweikhard, E.A. Cornell, *Phys. Rev. Lett.* **91**, 100402 (2003).